ERK2 but not ERK1 mediates HGF-induced motility in non-small cell lung carcinoma cell lines

Simone Radtke[1,2,*], Mina Milanovic[1,*], Carine Rossé[1,3], Manu De Rycker[1], Sylvie Lachmann[1], Andrew Hibbert[1], Stéphanie Kermorgant[2,‡] and Peter J. Parker[1,4,‡]

[1]London Research Institute, 44 Lincoln's Inn Fields, London WC2A 3LY, UK
[2]Centre for Tumour Biology, Barts Cancer Institute, Queen Mary University of London, John Vane Science Centre, Charterhouse Square, London EC1M 6BQ, UK
[3]Membrane and Cytoskeleton Dynamics Laboratory, CNRS, Paris Cedex, France
[4]Division of Cancer Studies, Guy's Campus, London SE1 1UL, UK

*These authors contributed equally to this work
‡Authors for correspondence (peter.parker@cancer.org.uk; s.kermorgant@qmul.ac.uk)

Accepted 11 March 2013
Journal of Cell Science 126, 2381–2391
© 2013. Published by The Company of Biologists Ltd
doi: 10.1242/jcs.115832

Summary

Aberrant signalling of receptor tyrosine kinases (RTKs), such as c-Met, the receptor for hepatocyte growth factor (HGF), has been implicated in the oncogenesis of various tumours including non-small cell lung carcinoma (NSCLC). Through its pro-migratory properties, c-Met has been implicated specifically in the process of tumour metastasis, demanding a better understanding of the underlying signalling pathways. Various players downstream of c-Met have been well characterised, including the extracellular-signal-regulated kinases (ERKs) 1 and 2. In a small interfering RNA (siRNA)-based high-throughput wound healing screen performed in A549 lung carcinoma cells, we identified ERK2 but not ERK1 as a strong mediator of HGF-induced motility. This finding was confirmed in several NSCLC cell lines as well as in HeLa cells. One known substrate for ERK kinases in cell migration, the focal adhesion protein paxillin, was also one of the hits identified in the screen. We demonstrate that HGF stimulation results in a time-dependent phosphorylation of paxillin on serine 126, a process that can be blocked by inhibition of the ERK1/2 upstream kinase mitogen-activated protein kinase/ERK kinase 1 (MEK1) or inhibition of glycogen synthase kinase 3 (GSK3). Further, we show that paxillin turnover at focal adhesions is increased upon stimulation by HGF, an effect that is dependent on serine residues 126 (GSK3 site) and 130 (ERK site) within paxillin. In line with the isoform-specific requirement of ERK2 for HGF-mediated migration in lung tumour cell models, ERK2 but not ERK1 is shown to be responsible for paxillin serine 126 phosphorylation and its increased turnover at focal adhesions.

Key words: HGF, c-Met, Motility, Wound healing, High-throughput screen, Signalling, siRNA, ERK2, Paxillin

Introduction

Cell migration is a fundamental process important for normal tissue homeostasis and is triggered by various environmental stimuli and their downstream signalling pathways, ultimately resulting in the rearrangement of the cytoskeleton, reorganisation of the microtubule organising centre, extension of membrane protrusions, adhesion to the substratum and generation of forces that physically move a cell (reviewed by Vicente-Manzanares et al., 2005). Aberrations in components of these signal transduction pathways can lead to tumour dissemination and invasion to surrounding tissues (reviewed by Friedl and Wolf, 2003), playing a major role in cancer development and progression.

Hepatocyte growth factor (HGF) can trigger cell migration through binding and activation of its only known receptor, c-Met, a receptor tyrosine kinase. The activated receptor serves as a docking site for various adaptor and signalling proteins, leading to the disassembly of adherens junctions, increased cell motility, survival and branching morphogenesis (Potempa and Ridley, 1998; Bowers et al., 2000; Zhang et al., 2002; Kermorgant and Parker, 2008). A role of c-Met has been observed in many human malignancies, including gastric and oesophageal carcinoma, medulloblastoma and Non Small Cell Lung Cancer (NSCLC) (Tong et al., 2004; Gao and Vande Woude, 2005; Miller et al., 2006). Importantly, HGF/c-Met are believed to play a major role in the progression to tumour metastasis (reviewed by Peruzzi and Bottaro, 2006; Sattler and Salgia, 2007) so that a detailed understanding of processes underlying c-Met-dependent cancer cell migration is important for providing opportunities for the development of new treatments for these diseases. Several downstream pathways of c-Met have been well characterised (reviewed by Trusolino et al., 2010); thus the importance of the ERK1/2 pathway in HGF-mediated cellular motility has been demonstrated in various cellular models (Tanimura et al., 1998; Zeigler et al., 1999; Karihaloo et al., 2001; Tanimura et al., 2002; Kermorgant et al., 2004; Menakongka and Suthiphongchai, 2010).

As c-Met overexpression, mutation or increased activation has been observed in NSCLC (reviewed by Sattler et al., 2011), we used the lung carcinoma cell line A549 to perform an siRNA-based wound healing screen in order to study the signalling pathways important for c-Met mediated migration and identified ERK2 but not ERK1 as one of the strongest hits. So far, the specific contribution of ERK1 and ERK2 has not been studied with respect to the HGF-signalling cascade. Here we show that HGF-induced motility is specifically mediated by ERK2 in several cell lines, and this finding correlated with the observation

Journal of Cell Science

that ERK2 but not ERK1 was required for the HGF-induced phosphorylation of the focal adhesion scaffold protein paxillin on serine 126, a site which has been described to be phosphorylated by glycogen synthase kinase (GSK) 3 upon priming of the adjacent serine 130 by ERKs (Cai et al., 2006). The important role of this phosphorylation in HGF-mediated migration was demonstrated by the finding that the siRNA-mediated depletion of endogenous paxillin results in a decrease in HGF-mediated migration, an effect which can be rescued by wild type paxillin but not a mutant in which serine 126 and the adjacent serine 130 are mutated to alanine. In line with the motility data, we can show that HGF stimulation results in an increased disassembly of paxillin-containing focal adhesions, an effect which can be inhibited by knockdown of ERK2 but not ERK1. Thus we propose that paxillin is an important mediator downstream of ERK2 in HGF-induced motility.

Results

Identification of ERK2 in an siRNA-based wound healing screen

We set up an siRNA-based high throughput wound healing assay using the A549 lung carcinoma cell model. Altogether, 1115 siRNA pools targeting the human kinome, a set of motor proteins as well as genes implicated in motility were transfected and a non-targeting control (NTC) siRNA and an siRNA against c-Met served as negative and positive controls respectively. An siRNA targeting the tyrosine kinase receptor Macrophage-stimulating protein receptor (MST1R), a c-Met paralog (Ronsin et al., 1993; Gaudino et al., 1994), was included as an additional control. A detailed schematic overview of how the Primary screen was carried out is depicted in supplementary material Fig. S1.

Cells transfected with non-targeting siRNA displayed roughly a twofold increase in motility speed upon HGF treatment, an effect which was almost completely abrogated upon transfection of the c-Met siRNA. In contrast, knockdown of the related receptor MST1R had a significant effect both on the basal and HGF-induced motility speed, retaining a twofold increase between the two wound healing speeds (Fig. 1A). To have a read out for the effect of the transfected siRNAs on the HGF-response, an HGF-induction score was calculated as exemplified in supplementary material Fig. S2. The normalised induction scores obtained for the negative and positive controls used are depicted in Fig. 1B. As expected, c-Met knockdown resulted in a strong decrease of the induction score to a value close to 0,

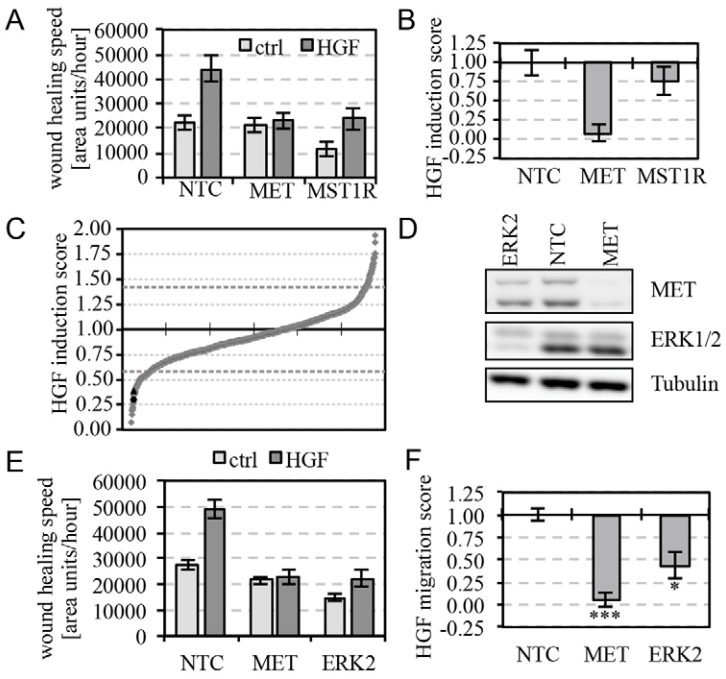

Fig. 1. High-throughput wound healing screen. A549 cells were transfected with 1115 Dharmacon siRNA pools directed against different genes. As a negative control a non-targeting siRNA was used (NTC), siRNAs targeting the HGF-receptor cMet (MET) and the related tyrosine kinase receptor Mst1R were used as additional controls. Wound healing assays were carried out 72 hours post transfection. Raw migration speeds were calculated for control treated and HGF-treated cells and using the two sets of raw migration data, HGF-induction scores were calculated as described in Material and Methods. (**A**,**B**) Negative and positive controls used in the screens. Raw migration speeds were calculated for control treated and HGF-treated cells. Averages and standard deviations calculated from all control values (A) and HGF-induction scores (B) obtained during the screen are depicted. (**C**) HGF-induction scores obtained during the primary screen. The obtained HGF-induction scores for all transfected siRNAs are shown in ascending order. Black dotted lines represent the thresholds used for classifying siRNAs that significantly increase or decrease the HGF-response. The black circle and the black triangle represent the values obtained for MET and ERK2, respectively, that were part of the assayed kinome library. (**D**) Knockdown efficiencies of transfected siRNAs. A549 cells were transfected with the siRNA pools as indicated and harvested 72 hours post transfection. Total cellular lysates were generated and knockdown efficiency was monitored by western blot analysis using the antibodies indicated. Representative blots are depicted. (**E**,**F**) siRNAs targeting MET and ERK2 strongly impair HGF-induced wound healing. A549 cells were transfected with the siRNA pools as indicated and 72 hours post transfection, wound healing assays were carried out. Average wound healing speeds were calculated for control-treated and HGF-treated cells (E). The HGF wound healing score was calculated from both values. Means ± s.e.m. derived from three independent experiments are depicted. Statistical significance was determined using paired Student's *t*-test (F); $*P<0.05$, $***P<0.001$.

whereas knockdown of MST1R only slightly affected the induction score. Fig. 1C displays the induction scores obtained during the primary screen in an ascending order. Thresholds were chosen as described in Materials and Methods. While 85 siRNAs were classified as negative regulators of the HGF-response, 43 siRNAs resulted in an increased HGF-response. Data obtained for all siRNAs is provided in supplementary material Table S1. MET kinase itself (black circle) and ERK2 (black triangle), which were both part of the library targeting the human kinome, came up among the top 20 hits, serving as a proof of principle that the screen was able to identify players involved in HGF-mediated signalling. These results could be confirmed in further experiments, where for both siRNA pools a good knockdown was observed by western blot (Fig. 1D). In wound healing experiments, ERK2 but not MET depletion resulted in a strong decrease of the basal wound healing speed (Fig. 1E). As expected, MET knockdown resulted in an almost completely abrogated HGF-induced migration, while ERK2 depletion reduced the HGF-induced migration by more than 50% (Fig. 1F).

Confirmation of the migratory phenotype in ERK2-depleted cells

In the primary screen, we used a wound healing assay to find players involved in HGF-induced cell migration. Not surprisingly given its role in the regulation of cell proliferation, we observed a strong effect of ERK2 depletion on cell viability (Fig. 2A). To confirm that the results obtained using the wound healing assays were not merely a consequence of reduced cell proliferation, we carried out live cell imaging followed by cell tracking to monitor single cell motility speed after siRNA knockdown. In Fig. 2B representative cell tracks in wounds of cells transfected with non-targeting control siRNA (NTC), MET siRNA or ERK2 siRNA are depicted. In NTC-transfected cells, HGF incubation led to approximately a twofold increase in the single cell motility speed, an effect which was almost completely abrogated by MET knockdown and also strongly inhibited (75%) by knockdown of ERK2 (Fig. 2C). Similar results were achieved using Transwell assays as a distinct migratory model (Fig. 2D), thus confirming the migratory phenotype observed in the wound healing assays.

Knockdown of ERK2 but not ERK1 has an effect on HGF-induced motility

While ERK2 was one of the strongest hits identified in this screen, intriguingly ERK1, the second ERK isoform, was not identified as a hit. To assess the validity of this finding, we compared the effect of ERK2 and ERK1 knockdown side by side. Silencing of both ERK2 and ERK1 resulted in an efficient knockdown as evidenced by western blot analysis (Fig. 3A) and depletion of both ERK isoforms had a very similar effect on cell viability (Fig. 3B). Both ERK1 and ERK2 depletion resulted in a significantly reduced basal motility with a consistently greater effect of ERK1 knockdown (Fig. 3C, light grey bars). However by contrast, ERK2 knockdown alone strongly impaired the HGF response, while ERK1 silencing did not, with HGF still able to induce a strong increase in wound healing speed (Fig. 3C, right panel). Interestingly, the MEK1 inhibitor U0126 gave similar results as the single knockdown of ERK2 (Fig. 3D). The specific role of ERK2 in HGF-mediated motility was not restricted to A549 cells, since also in CALU-1 and SKMES-1 lung carcinoma

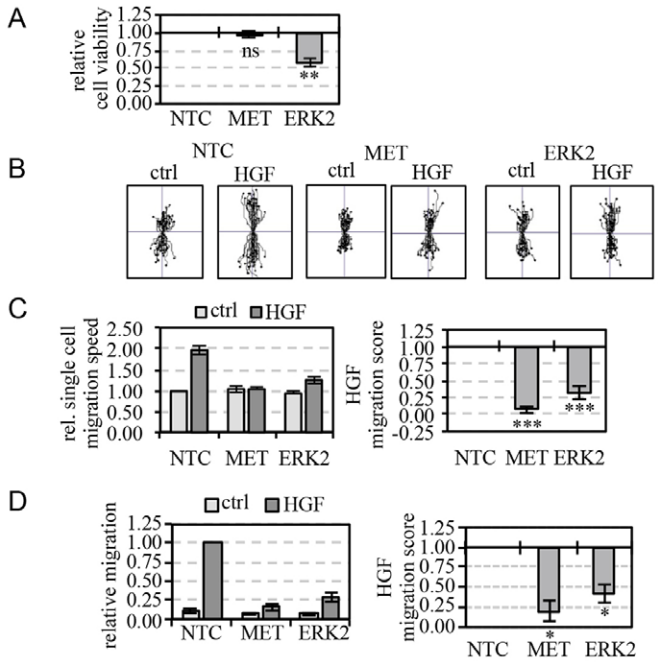

Fig. 2. Validation of the migratory phenotype. (**A**) Knockdown of ERK2 significantly reduces cell viability. Cell viability of transfected cells was assayed using CellTiter-glo as described in Materials and Methods. Values were normalised to data obtained from NTC transfected cells. Means ± s.e.m. derived from four independent experiments are depicted. (**B**,**C**) Live cell imaging and single cell tracking. Transfected A549 cells were grown to confluency and 72 hours post transfection, wounding was performed, cells were incubated in medium containing 0.5% FCS with or without HGF and live cell imaging was carried out for 12 hours. From the resulting pictures, movies were generated and at least 20 cells per movie were tracked and cell tracks analysed as described in Materials and Methods. For each condition, median single cell motility speeds were calculated from at least 40 cell tracks per experiment. Representative tracks from one experiment are depicted (B). Average single cell speed values and the resulting HGF migration scores obtained from four independent experiments are depicted (C). (**D**) Transwell assays. 72 hours post transfection, cells were trypsinised and plated onto 24-well transwell dishes or normal 24-well tissue culture plates in duplicate. After incubation for 3 hours with or without HGF, the cell numbers of plated cells and of cells that had migrated through the transwells were estimated using CellTiter-glo and the percentage of migrated cells was calculated. The average value obtained from NTC transfected, HGF-treated cells was set to 1. Means ± s.e.m. obtained from three independent experiments are depicted in the left diagram; the resulting average HGF migration scores are depicted in the right diagram. In all cases, statistical significance was determined by paired Student's *t*-test; $*P<0.05$, $**P<0.01$, $***P<0.001$; ns, not significant.

cell lines as well as in HeLa cells, HGF-induced cell motility was affected by knockdown of ERK2 but not ERK1 (Fig. 3E).

Paxillin is required for HGF-mediated migration

Various substrates of the ERK kinases have been reported to play a role in cellular migration, including the focal adhesion protein paxillin, which has been shown previously to be important for HGF-induced migration (Liu et al., 2002; Ishibe et al., 2003; Ishibe et al., 2004). Interestingly, paxillin was another strong hit in the wound healing screen we performed and indeed this data could be confirmed in cell tracking experiments both in A549 and in HeLa cells (Fig. 4A). Knockdown of paxillin did not affect

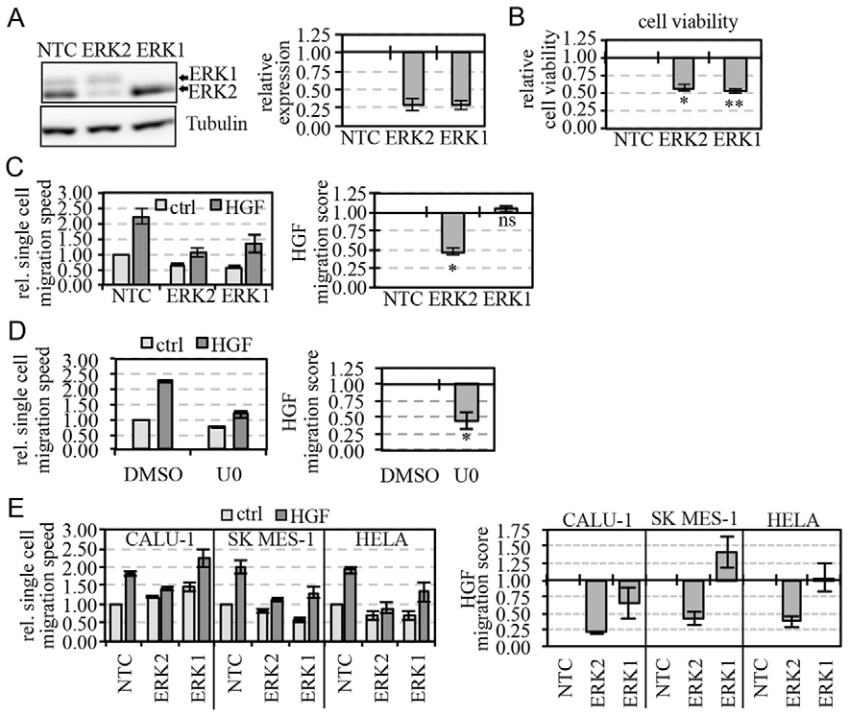

Fig. 3. ERK2 but not ERK1 is essential for HGF-induced wound healing. (**A**) Knockdown efficiency of siRNAs used. A549 cells were transfected with the siRNA pools indicated and 72 hours post transfection total cellular lysates were generated and expression of ERK1 and ERK2 was monitored by western blot analysis. A representative blot is depicted in the left panel. Blots were quantified as described in Materials and Methods and the relative expression was calculated. Means ± s.e.m. derived from three independent experiments are displayed. (**B**) ERK2 and ERK1 knockdown have a similar effect on cell viability. A549 cells were transfected with the indicated siRNAs and harvested 72 hours post transfection. Cell viability was assayed as described in Materials and Methods. Means ± s.e.m. from three independent experiments are depicted. (**C**) ERK2 but not ERK1 knockdown affects HGF-induced motility. A549 cells were transfected with the siRNAs indicated and 72 hours post transfection, cell wounding and live cell imaging were performed. Cell tracking was carried out and single cell motility speeds (left panel) as well as HGF migration scores (right panel) were calculated as described in Materials and Methods. Means ± s.e.m. derived from three independent experiments are depicted. (**D**) Effect of MEK1 inhibition. A549 cells were treated with DMSO or U0216 (U0) for 20 minutes before wounding was carried out. Cell motility was monitored by videomicroscopy. Cell tracking was carried out and HGF migration scores were calculated from the obtained single cell motility speeds as described in Materials and Methods. Average normalised single cell motility speeds as well as HGF migration scores are depicted. To determine statistical significance, paired Student's *t*-test was used. (**E**) ERK2 is specifically needed for HGF-induced wound healing in various cell lines. The indicated siRNAs were transfected into HeLa, CALU-1 and SKMES-1 cells. At 72 hours post transfection, cells were wounded and wound healing was monitored using videomicroscopy. Cell tracking was carried out and HGF migration scores were calculated from the obtained single cell motility speeds as described in Materials and Methods. Average HGF-migration scores are depicted. In all cases, statistical significance was determined using paired Student's *t*-test; $*P<0.05$, $**P<0.01$.

HGF-induced MET or ERK phosphorylation in A549 cells (Fig. 4B) or HeLa cells (data not shown). To further investigate the role of paxillin in HGF-mediated motility, we monitored paxillin turnover in HeLa cells by total internal reflection fluorescence (TIRF) microscopy. When analysing focal adhesions containing GFP-tagged paxillin over time as described (Berginski et al., 2011), we saw an increase of focal adhesion disassembly rates upon HGF stimulation (Fig. 4C). Paxillin turnover has been shown to be regulated by phosphorylation (Webb et al., 2004; Berginski et al., 2011) and indeed, HGF stimulation resulted in an increase in the phosphorylation of serine 126 in paxillin, an effect which was maximal after about 2 hours of HGF stimulation (Fig. 4D). Serine 126 has been described to be phosphorylated by glycogen synthase kinase 3 (GSK3) upon priming of the adjacent serine 130 by ERK (Cai et al., 2006). Consistent with this, HGF-mediated phosphorylation of serine 126 was abrogated both by incubation with the MEK1 inhibitor U0126 or the GSK3 inhibitor IX (Fig. 4E). To further investigate the role of these two phosphorylation sites in HGF-mediated migration, we constructed GFP-tagged paxillin where both serine 126 and serine 130 were mutated to alanine (GFP-PaxAA). These constructs were transfected into HeLa cells and adhesion turnover was monitored by TIRF microscopy. As seen before, HGF resulted in an increase of the disassembly rate of focal adhesions, an effect which was strongly inhibited in focal adhesions containing the paxillin mutant (Fig. 4F). Furthermore, in HeLa cells, siRNA-mediated knockdown of endogenous paxillin by a single oligo resulted in a significantly reduced HGF-mediated migration as monitored by live cell imaging, an effect which could be rescued by overexpression of GFP-tagged wild-type (wt) paxillin but not the mutant GFP-PaxAA (Fig. 4G).

ERK2 knockdown results in diminished HGF-induced paxillin phosphorylation and turnover

Given the important role of paxillin phosphorylation in HGF-mediated migration, we next monitored phosphorylation of paxillin upon knockdown of either ERK1 or ERK2.

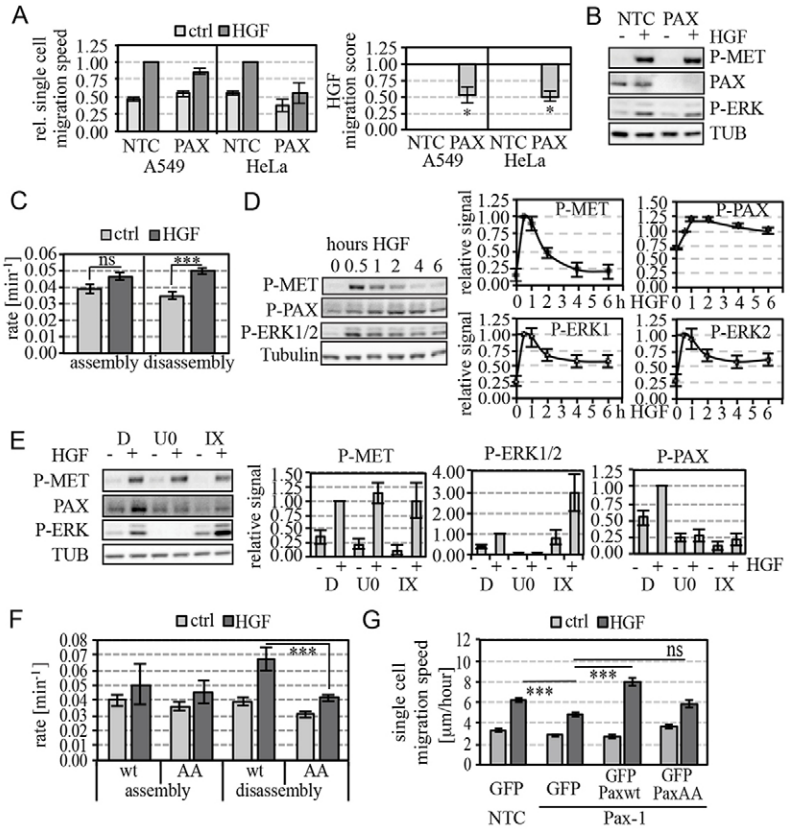

Fig. 4. Paxillin is required for HGF-induced migration and is phosphorylated upon HGF treatment. (**A**) Paxillin depletion results in reduced cell motility upon HGF treatment. A549 cells and HeLa cells were transfected with the siRNAs indicated and 48 hours post transfection cell wounding and live cell imaging was performed. Cell tracking was carried out and single cell motility speeds as well as HGF migration scores were calculated as described in Materials and Methods. Average normalised single cell motility speeds are shown in the left panel; HGF migration scores are shown in the right panel. Means ± s.e.m. derived from four independent experiments are depicted. Statistical significance was determined using paired Student's *t*-test. (**B**) Paxillin depletion does not affect the HGF-induced phosphorylation of MET and ERK1/2. A549 cells were transfected with control siRNA (NTC) or siRNA targeting paxillin. At 48 hours post transfection, cells were treated for 2 hours with HGF or left untreated, total cellular lysates were generated and analysed by western blot as indicated. Representative blots are shown. (**C**) HGF treatment increases the paxillin turnover in HeLa cells. HeLa cells transiently expressing GFP-tagged paxillin were cultured in 10% FCS or 10% FCS supplemented with HGF and monitored over 30 minutes using TIRF microscopy. The resulting movies were used to calculate the assembly and disassembly rates of paxillin containing focal adhesions, as described in the Materials and Methods. At least 10 movies per condition were analysed. Statistical significance was determined using the unpaired Student's *t*-test. (**D**,**E**) HGF-mediated paxillin phosphorylation on serine 126 is ERK- and GSK3-dependent. Cells were treated with HGF for the indicated time points and total cellular lysates were generated (D). For inhibitor experiments, cells were pretreated with DMSO, U0216 (U0) or GSK3 inhibitor IX (IX) for 20 minutes and then treated with HGF or left untreated for 2 hours and total cellular lysates generated (E). Lysates were analysed by western blot with the antibodies indicated. Representative blots are shown in the left panel. Blots were quantified using ImageJ software and values normalised to those obtained for tubulin. Average normalised values from three independent experiments are depicted. (**F**) Altered HGF-induced disassembly rates in cells expressing GFP-paxillin-AA. HeLa cells transiently expressing GFP-tagged wild-type paxillin (wt) or mutated paxillin (AA) were cultured in 10% FCS or 10% FCS supplemented with 50 ng/ml HGF and monitored over 30 minutes using TIRF microscopy. The resulting movies were used to calculate the assembly and disassembly rates of paxillin-containing focal adhesions, as described in the Materials and Methods. At least 10 movies per condition were analysed. (**G**) GFP-paxillin-wt but not GFP-paxillin-AA can rescue the HGF-induced migration in HeLa cells depleted of endogenous paxillin. HeLa cells were transfected with non-targeting control siRNA or an siRNA oligo targeting paxillin and 24 hours post transfection were further transfected with a cDNA for GFP, GFP-paxillin-wt or GFP-paxillin-AA. The next day, a wound healing assay was performed and cell migration was monitored by live cell imaging and single cell migration speeds determined by cell tracking. For each condition, six movies were analysed. Average single cell migration speeds are depicted. Statistical significance was determined using one-way Anova; *$P<0.05$, ***$P<0.001$; ns, not significant.

Interestingly, in cells transfected with siRNA against ERK1, HGF was still able to cause an increase in paxillin phosphorylation, however, this effect was strongly inhibited when ERK2 was depleted by siRNA (Fig. 5A). Experiments using the deconvoluted ERK2 siRNA pool corroborated these findings (supplementary material Fig. S3). Furthermore, this effect was not restricted to A549 cells, as also in CALU, SKMES and HeLa cells, ERK2 knockdown led to a strong decrease in HGF-mediated paxillin phosphorylation (supplementary material Fig. S4).

It has been shown that the phosphatidylinositide 3-kinase (PI3K)/AKT-mediated serine phosphorylation of GSK3 negatively regulates its activity (Wang et al., 1994; Cross et al., 1995). Indeed we saw an increase of AKT and GSK3 phosphorylation upon HGF treatment (supplementary material Fig. S5), and GSK3 phosphorylation could be almost completely prevented by preincubation with the PI3K inhibitor LY294002 (supplementary material Fig. S5B). To exclude the possibility that the effect of ERK2 knockdown on paxillin phosphorylation

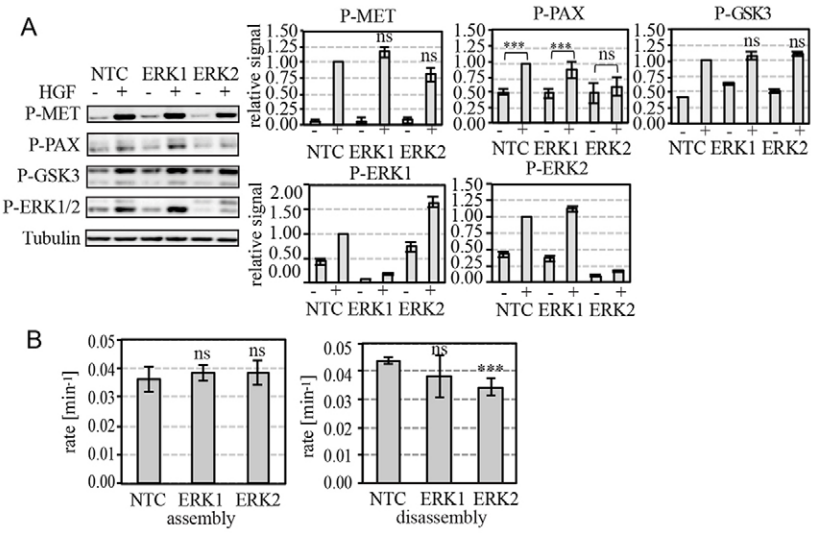

Fig. 5. ERK2 knockdown inhibits HGF-mediated paxillin phosphorylation and decreases paxillin turnover. (**A**) ERK2 knockdown prevents HGF-induced paxillin phosphorylation. A549 cells were transfected with control siRNA (NTC) or siRNA targeting ERK2 or ERK1. At 48 hours post transfection, cells were treated for 2 hours with HGF or left untreated, total cellular lysates were generated and analysed by western blot as indicated. Representative blots are shown on the left panel. Blots were quantified using ImageJ software and values normalised to those obtained for tubulin. Average normalised values are depicted. To determine statistical significance, two-way Anova was carried out, followed by Bonferroni post hoc test. (**B**) ERK2 knockdown decreases the paxillin disassembly rate in HGF-treated HeLa cells. HeLa cells depleted of ERK1 or ERK2 by siRNA for 48 hours and transiently expressing GFP-tagged paxillin were cultured in 10% FCS supplemented with HGF and monitored over 30 minutes using TIRF microscopy. The resulting movies were used to calculate the assembly and disassembly rates of paxillin containing focal adhesions, as described in the Materials and Methods. At least 10 movies per condition were analysed. Statistical significance was determined using one-way Anova followed by Bonferroni post hoc test; ***$P<0.001$; ns, not significant.

could be due to altered GSK3 activity, we therefore also monitored GSK3 phosphorylation, however, there was no difference in the HGF-mediated GSK3 phosphorylation upon ERK2 knockdown (Fig. 5A).

Finally, when monitoring the effect of ERK1 and ERK2 knockdown on paxillin turnover in HGF treated HeLa cells, we saw that assembly rates were not affected by either ERK1 or ERK2 knockdown, whereas ERK2 but not ERK1 knockdown resulted in a significant decrease in the rate of paxillin disassembly (Fig. 5B). We conclude that HGF via ERK2 induces phosphorylation of paxillin, thus mediating an increase both in paxillin turnover at focal adhesions and cell migration.

Overexpression of ERK2 but not ERK1 can efficiently rescue the effects of siRNA-mediated knockdown of endogenous ERK2

The fact that knockdown of ERK2 but not ERK1 resulted in loss of HGF-induced migration and paxillin phosphorylation could theoretically be explained by the fact that ERK2 is the prominent isoform expressed. We therefore tested whether the effect of the knockdown of endogenous ERK2 could be rescued by either overexpression of ERK1 or ERK2. A549 cells were transfected with a single siRNA oligonucleotide targeting ERK2 (E2-1), and 24 hours later, cDNA for either HA-tagged ERK1 or ERK2 was transfected; an empty vector served as a negative control. Paxillin phosphorylation and ERK activation were monitored by western blotting. Both ERKs were expressed to a similar extent (Fig. 5A, left panel), and both ERK1 expression and ERK2 expression could rescue overall ERK-activation to a similar extent (Fig. 5A, upper graph). However, only ERK2 but not ERK1 overexpression could rescue the phosphorylation of paxillin (Fig. 5A, lower graph). Similarly, ERK2 and not ERK1 expression resulted in the rescue of HGF-induced single cell motility (Fig. 5B). To assess these findings in non-lung tumour cells, we also carried out rescue experiments in HeLa cells. In these experiments ERK1 was much more effectively expressed than ERK2, and while both ERK isoforms were able to rescue the HGF-mediated paxillin phosphorylation to some extent, ERK2 was more efficient than ERK1 in doing so, such that there is an almost twofold relative efficiency of activated ERK2 compared to activated ERK1 in mediating the HGF-induced paxillin phosphorylation (supplementary material Fig. S6A). In line with these findings, when monitoring the ability of ERK1 and ERK2 to rescue HGF-mediated cell motility, we similarly noted a greater ability of ERK2 than ERK1 to do so (supplementary material Fig. S6B). A schematic model summarising our findings is displayed in Fig. 6C. We conclude that HGF can regulate paxillin phosphorylation via its effects on GSK3 and ERK2. Our finding that ERK2 is the dominant ERK isoform in mediating paxillin phosphorylation can explain the strong impact of ERK2 but not ERK1 knockdown on Paxillin turnover and cell migration.

Discussion

Understanding the detailed signalling pathways required for HGF-mediated migration is of great interest for better understanding and therefore selectively targeting aberrant signalling of c-Met in cancer metastasis. In performing an siRNA based high throughput wound healing screen in the NSCLC cell line A549, one of the strongest hits identified was ERK2, inhibiting the HGF-mediated migration consistently by more than 50%. ERK1 and 2 have been implicated in migration in various cell types, in response to different matrix proteins, various growth factors and other stimuli (Karihaloo et al., 2001; Huang et al., 2004). Therefore, the finding that ERK2 is one of

Journal of Cell Science

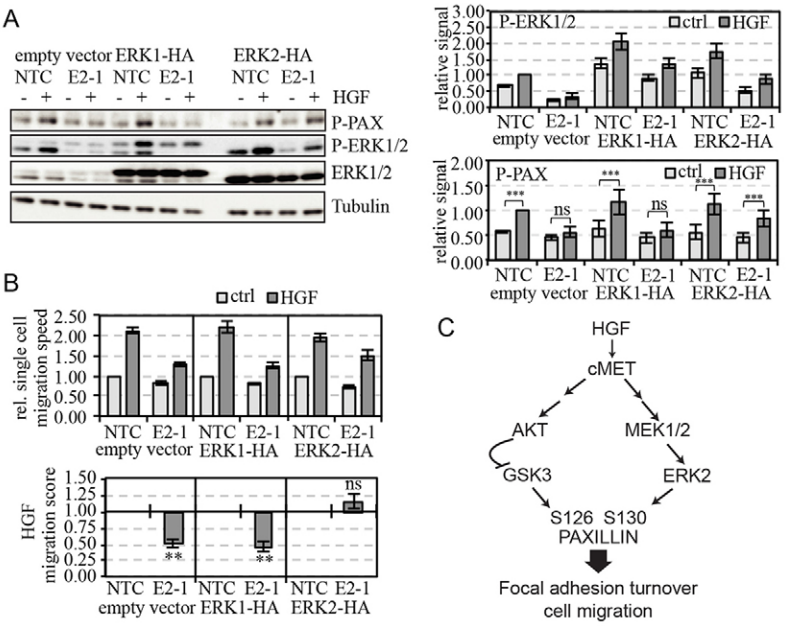

Fig. 6. ERK2 but not ERK1 overexpression can rescue the effect of siRNA-mediated knockdown of endogenous ERK2. A549 cells were transfected with control siRNA (NTC) or a single siRNA oligonucleotide targeting ERK2 (E2-1). 24 hours post transfection, cDNAs coding for HA-tagged ERK1 or ERK2 or empty vector were transfected. Experiments were carried out the next day. (**A**) HGF-mediated paxillin phosphorylation on serine 126 can be rescued by ERK2. Cells were treated with HGF for 2 hours and total cellular lysates were generated. Lysates were analysed by western blot with the antibodies indicated. Representative blots are shown in the left panel. Blots were quantified using ImageJ software and values were normalised to values obtained for tubulin. Average normalised values derived from five independent experiments are depicted. To determine statistical significance, two-way Anova was carried out, followed by Bonferroni post hoc test. (**B**) ERK2 but not ERK1 overexpression can rescue the HGF-induced increase in single cell motility. Cell wounding, live cell imaging and cell tracking were carried out and single cell motility speeds as well as HGF migration scores were calculated as described in Materials and Methods. Average normalised single cell motility speeds are shown in the upper panel, HGF migration scores are shown in the lower panel. Means ± s.e.m. derived from four independent experiments are depicted. Statistical significance was determined using the paired Student's *t*-test. (**C**) Schematic overview of the cMet–paxillin signaling axis. The dominant players involved in regulation of paxillin phosphorylation upon HGF are displayed. $^{**}P<0.01$, $^{***}P<0.001$; ns, not significant.

the strongest hits isolated from the screen provides a proof-of-principle in terms of screen validity. However it is striking that in the screen, only ERK2 but not ERK1 was found to affect HGF-induced migration. While a role for the ERK1/2 pathway in HGF-mediated motility has been shown before, most studies related to ERK1/2 signalling have made no functional distinction between the two isoforms and whether ERK1 and ERK2 play similar or distinct roles in HGF dependent motility has remained unknown. The evidence here demonstrates that it is ERK2 and not ERK1 that plays a role downstream of MET in lung tumour models and that there is a strong bias towards ERK2 in other cell types tested.

Until recently isoform specificity of ERKs has not been widely addressed. Indeed several studies have shown a redundant function of ERK1 and ERK2 in cell proliferation (Srinivasan et al., 2009; Voisin et al., 2010). Likewise, in a mouse model of K-Ras induced NSCLC, elimination of individual ERK kinases resulted in a similar small decrease of K-Ras induced oncogenesis, while only elimination of both ERK1 and ERK2 impaired tumour development (Blasco et al., 2011). In line with these publications, when monitoring cell viability, we also find a similar effect upon knockdown of either ERK isoform. In contrast to such a redundant function of both ERK isoforms, there are recent studies that have identified some isoform specific functions. Thus, ERK1 and ERK2 have been demonstrated to fulfil different roles in Ras-dependent signalling (Vantaggiato et al., 2006) and long-term survival of hepatocytes (Frémin et al., 2009). While some differences in ERK isoform signalling have been attributed to differences in the N-terminal domain of both isoforms (Marchi et al., 2008), other studies have shown that differences might be due to the expression level of each isoform (Lefloch et al., 2008; Lefloch et al., 2009). Indeed ERK2 is expressed to a much higher level than ERK1 in all of the cell lines we examined, although some properties of these cells such as basal migration rates were more sensitive to ERK1 knockdown than to ERK2 knockdown. Notwithstanding this preferential effect of ERK1, to examine whether our findings are due to the fact that ERK2 is the prominent isoform, we also carried out rescue experiments using HA-tagged ERK constructs. In A549 cells, only ERK2 but not ERK1 could rescue the knockdown of endogenous ERK2. Similarly, while both ERK isoforms were able to rescue the knockdown of ERK2 in HeLa cells, ERK2 was much more efficient in doing so.

Interestingly it has recently been found that ERK2 but not ERK1 overexpression induced epithelial-to-mesenchymal transformation in MCF-10A cells (Shin et al., 2010). Likewise, in MDA-MB-231 cells, ERK2 but not ERK1 knockdown inhibits cell invasiveness (von Thun et al., 2012). Consistent with this, our results suggest that also in case of c-Met driven tumour metastasis, ERK2 might be the dominant ERK isoform.

Many cellular substrates have been reported to be phosphorylated by ERKs, including both nuclear and cytoplasmic proteins. One of the known ERK substrates shown

Journal of Cell Science

Journal of Cell Science

to play a role in cellular motility is paxillin (reviewed by Brown and Turner, 2004) and paxillin has been implicated in cell spreading and morphogenesis upon HGF treatment (Liu et al., 2002; Ishibe et al., 2003; Ishibe et al., 2004). Of note, paxillin was another strong hit identified in our screen, and we could confirm a role for paxillin in HGF-mediated motility in cell tracking experiments both in A549 and HeLa cells (Fig. 4A). Various phosphorylation sites have been identified in paxillin (Webb et al., 2005) and we find an HGF-induced phosphorylation of paxillin on serine 126. The HGF-mediated phosphorylation of paxillin on Tyrosine 118 and serine 83 has been demonstrated before (Liu et al., 2002; Ishibe et al., 2003; Ishibe et al., 2004). However, the role of serine 126 in HGF-induced motility has not been studied so far. Of note paxillin phosphorylation at this site is maximal at around two hours of HGF stimulation and therefore peaks slightly later than P-MET and P-ERK, a finding we also could reproduce in other cell lines (data not shown). This small delay can probably be explained by the fact that serine 126 is not a direct substrate of ERK but in fact phosphorylation of this site has been attributed to the kinase GSK3, which can only efficiently phosphorylate this site upon priming phosphorylation of the upstream serine 130 by ERK (Cai et al., 2006). Using inhibitors against MEK1 and GSK3, we can confirm these findings in A549 cells.

GSK3 activity has been shown to be regulated by serine and tyrosine phosphorylation (Wang et al., 1994). Thus phosphoinositide 3-kinases (PI3-K)/AKT-mediated phosphorylation of serine 9 inhibits the activity of GSK3β (Cross et al., 1995), whereas phosphorylation of tyrosine 216 positively affects its activity (Wang et al., 1994). HGF is a strong inducer of AKT activity (reviewed by Trusolino et al., 2010), therefore not surprisingly, we find an increase in phosphorylation of the inhibitory serine 9 in GSK3β peaking at 1 hour of HGF stimulation. There is also a small but reproducible increase in phosphorylation of tyrosine 216, which plateaus between 1 and 4 hours of HGF stimulation (supplementary material Fig. S5). The transient phosphorylation of serine 9 can explain the delayed kinetics of paxillin Serine 126 phosphorylation upon HGF stimulation; indeed when AKT-mediated GSK3 phosphorylation is prevented by the PI3K inhibitor LY294002, we find a shift in the kinetics to an earlier timepoint (supplementary material Fig. S5B), thus HGF-mediated paxillin phosphorylation seems to be tightly regulated via the combined outputs of the AKT and ERK2 signaling pathways.

We show that phosphorylation of serine 126 can be blocked by knockdown of ERK2 but not ERK1 (Fig. 5A), a finding which we can reproduce in several cell lines (supplementary material Fig. S4). Of note, in Calu as well as in HeLa cells, ERK1 knockdown results in a small reduction in paxillin phosphorylation, however, the effect of ERK2 knockdown is much more pronounced. Consistent with these findings, ERK2 is significantly more efficient than ERK1 in rescuing the diminished paxillin phosphorylation seen in cells transfected with siRNA targeting ERK2 (Fig. 6A; supplementary material Fig. S6), thus correlating very well with the motility data. Indeed, the relevance of phosphorylation of serine 126 and adjacent serine 130 during cell migration was demonstrated by the fact that the decreased HGF-induced motility seen upon paxillin knockdown can be rescued by wild-type paxillin but not by a mutant where the GSK3 and ERK sites have been mutated to alanine (Fig. 4G).

We speculate that the ERK2-specific regulation of HGF-induced motility is due in part to specific ERK2-mediated paxillin phosphorylation, which would in turn affect focal adhesion dynamics as demonstrated in a different motility model (Boeckeler et al., 2010). Indeed we find that HGF-treatment results in an increase of the disassembly rate of paxillin-containing focal adhesions (Fig. 4C). This effect is blocked in a mutant paxillin in which serine 126 and serine 130 have been mutated to alanine and hence can no longer be phosphorylated at these sites (Fig. 4F), and ERK2 but not ERK1 knockdown significantly decreases the disassembly rate of adhesions in HGF treated A549 cells (Fig. 5B).

Aberrant c-Met signalling has been implicated in the oncogenesis of NSCLC (reviewed by Cipriani et al., 2009), where c-Met overexpression correlates with metastatic tendency and poor prognosis and is found in a high proportion of NSCLCs as demonstrated by immunohistochemistry (Ma et al., 2005; Ma et al., 2008). In 5% of NSCLC, c-Met overexpression is due to gene amplification (Cappuzzo et al., 2009) and, interestingly, c-Met amplification has been associated with resistance of NSCLC to gefitinib, an EGFR targeted therapy (Cappuzzo et al., 2009). Interestingly, paxillin has also recently been found to be upregulated in NSCLC, correlating with a poor prognosis (Jagadeeswaran et al., 2008; Wu et al., 2010; Mackinnon et al., 2011) and it has been reported that there is a high correlation of paxillin and MET gene copy numbers in NSCLC (Jagadeeswaran et al., 2008). Therefore, a better understanding of the c-Met-paxillin signalling axis in HGF-mediated motility is important for targeting this pathway in NSCLC and our findings that specifically ERK2 but not ERK1 is required in this pathway may have important implications for helping to design and apply specific therapies in future.

Materials and Methods

Cell culture

Cells were obtained from Cancer Research UK London Research Institute's Cell Services and cultured at 37°C in a humidified 10% CO_2 atmosphere. Cells were cultivated in GIBCO® GlutaMAX™ media (Invitrogen) supplemented with 10% Certified FBS (Invitrogen) and 50 μg Penicillin-Streptomycin (Invitrogen).

HGF was purchased from R&D Systems and used routinely at 10 ng/ml, with the exception of HeLa cells, which were treated with 40 ng/ml. U0126 was from Cell Signaling and used at 10 μM. GSK3 inhibitor IX was purchased from Santa Cruz Biotechnology and used at 5 μM. LY294002 was from Sigma-Aldrich and used at 10 μM.

siRNA libraries

siRNA libraries used in the primary screen were obtained from Dharmacon. The complete list of genes targeted, siRNAs used and Entrez IDs can be found in supplementary material Table S1.

siRNA and cDNA transfections

For the primary screen, each siRNA was transfected in six replicate wells on 96-well plates with Hiperfect transfection reagent (Qiagen), using a reverse transfection protocol according to the manufacturer's instructions. 20 μl transfection mixture containing both the siRNA and 0.5 μl hiperfect diluted in Optimem were mixed with 80 μl cell suspension to give a final concentration of 10 nM siRNA and 8×10^3 cells per well. Growth medium was replaced 24 hours later, and cells were incubated for a further 48 hours. Unless stated otherwise, experiments were carried out 72 hours post transfection. For some experiments, cells were transfected on 24-well, 12-well or 6-well plates, using the equivalent cell densities, amount of Hiperfect per ml medium and final siRNA concentrations as for the transfection of 96-well plates. SK MES-1 cells were transfected using Hiperfect or RiboJuice (Novagen) according to manufacturer's instructions. HeLa cells were transfected using lullaby (OZ biosciences). For transfections of cDNA into A549 and HeLa cells, the LTX reagent (Invitrogen) was used according to the manufacturer's instructions.

Generation of cDNA constructs

The C-terminal HA tag as well as NheI and XbaI restriction sites were inserted into mouse ERK2 and human ERK1 cDNA respectively by standard PCR techniques

Journal of Cell Science

using appropriate oligonucleotides. The PCR products were inserted into the pcDNA3 vector (Invitrogen) using the in-Fusion® HD Cloning Kit (Clontech). The GFP-paxillin AA mutant was generated using the QuikChange Site-directed Mutagenesis kit (Stratagene) with chicken GFP-paxillin as a template, and two oligos containing the double mutation Ser126Ala/Ser130Ala. The validity of all resulting constructs was confirmed by sequencing.

High-throughput wound healing assay

Wound healing assays were carried out on 96-well clear bottom plates 72 hours post transfection. In order to minimise edge effects, only the 48 central wells of each 96-well plate were used. In the primary and secondary screens, 40 library siRNAs and 8 control siRNAs were transfected per plate, including four non-targeting control siRNAs (NTC), two siRNAs targeting cMet (MET) and two siRNAs targeting MST1R. The confluent cell monolayer was wounded using a 96 well stainless steel pin tool (V&P Scientific, Inc.), which introduced a single horizontal wound in each well. After wounding, cell debris was aspirated, cells were washed once in migration medium (GIBCO® GlutaMAX™ supplemented with 0.5% FBS), and medium was replaced with migration medium alone in order to measure basal migration, or migration medium supplemented with 10 ng/ml HGF. Triplicate wells were used for both conditions. A picture of each well was acquired using the semi-automated imaging system, Discovery-1. Cells were placed at 37℃, 10% CO_2 atmosphere and allowed to migrate for 6 hours, after which a second picture of the same area of the wound was taken. Representative grey scale pictures of control transfected cells treated with 0.5% FBS alone or with 0.5% FBS and HGF are depicted in supplementary material Fig. S1.

Calculation of wound healing speeds

Two grey-scale images were obtained per well using the Discovery-1 imaging system; one at time point zero and one at 6 hours. Resulting images were analysed using a customised MetaMorph (Molecular Devices) journal, which allowed us to quantify the area surrounding the wound, generating two area values for each well. The rate of wound closure per hour was calculated based on the difference in wound size during the six hour migration time course. Mean values and s.e.m.s were calculated for basal and HGF-induced migration (supplementary material Fig. S1, column graphs, light and dark blue bars, respectively).

Calculation of HGF induction scores

Values from each of the three replicates for both basal and HGF-induced migration were averaged to give a single value per replicate. The original data from one half plate (48 siRNAs) is displayed in supplementary material Fig. S2A. Plotting basal migration speed values (x-axis) versus HGF-induced migration speed data (y-axis) on a dot plot graph reveals a strong correlation between the two data sets (supplementary material Fig. S2B). Using this correlation between these two data sets, for each observed basal motility value, a corresponding expected HGF-motility value was calculated. Most observed HGF-motility values are very close to the calculated, expected values. However, a subset of hits affect the ligand-stimulated migration more or less strongly than they affect the basal migration, therefore decreasing or increasing the fold migration. These hits can be distinguished from the rest of the values by appearing in the dot plot diagram significantly above or below the correlation line, as exemplified in supplementary material Fig. S2B by the MET controls (red crosses), and MET present in the library (circled). In contrast, the points representing the non-targeting negative controls (filled dark grey circles) and MST1R (red boxes) lie on the correlation line. To quantify this effect for each siRNA, an HGF induction score was calculated using the formula depicted in supplementary material Fig. S2C, which takes into account the observed basal and HGF wound healing speeds as well as the expected HGF wound healing speed. An induction score of 1 represents normal HGF induction, values below 1 represent reduced HGF induction and values above 1 represent increased HGF induction. The bar diagram in supplementary material Fig. S2D displays the induction scores calculated from the values depicted in supplementary material Fig. S2A. Again, the value for c-Met which was present on this exemplar subplate, is boxed. This analysis was carried out separately for each transfected library subplate and finally, all induction scores obtained during the primary screen were normalised to the average of all induction scores obtained from cells transfected with non targeting control siRNA (NTC).

MTT assays

MTT [3-(4, 5 dimethylthiazol-2-yl)-2,5-diphenyltetrazolium bromide; Sigma] powder was dissolved in PBS to a final concentration of 5 mg/ml. 10 µl was added to each well of a 96-well plate, which contained the wounded cell monolayer in 100 µl cell culture medium. Cells were incubated at 37℃, 10% CO_2 for 45 minutes. Medium was aspirated and formazan crystals were dissolved in 50 µl DMSO (Sigma). After 10 minutes incubation at 37℃, plates were placed on a shaker for an additional 10 minutes. Absorbance was read on a SpectraMax Plus plate reader (Molecular Devices), coupled to SoftMax Pro 4.7 software. The four values obtained were averaged to give one MTT value per transfected siRNA.

Nuclei count

After carrying out the wound healing assay, transfected cells were fixed using 3.7% formaldehyde. Fixed cells were stained with Hoechst 33342 and Alexa Fluor 555-coupled phalloidin and washed three times with PBS. For each 96-well, three pictures were taken of the centre of the well including the wound edge using Cellomics® ArrayScan® and subsequently analysed with ThermoFisher Scientific-designed BioApplications software. Obtained values for nuclei counts were normalised to the values obtained for phalloidin that reflects the cell growth area within each picture. The obtained values were averaged to generate one nuclei count value per transfected siRNA.

Normalisation of primary data

Average values for basal motility, nuclei count and MTT obtained from each transfected subplate (40 library values and 8 control values) were normalised using the plate median (calculated from 40 library values). All values were then further normalised to the average value obtained from all cells transfected with non targeting control siRNA. To obtain a viability score, the MTT scores and Nuclei count scores thus obtained were averaged. For each readout, thresholds were defined based on the normal distribution of the values obtained for NTC-transfected cells, using the calculated average ± 2.576 ($P=0.005$) standard deviations as cut-off points.

Time-lapse video microscopy

Transfected cells growing on 96-well plates were wounded 60 hours post transfection, and cell debris was washed once with migration medium, after which migration medium alone, or migration medium supplemented with 10 ng/ml HGF was added. The images were obtained using the automated invert Nikon Eclipse TE2000-E microscope equipped with 10×Nikon Plan Fluor objective and Nikon iXon^{EM} camera (Andor™ Technology). Plates were left overnight in an incubator box, which ensured equilibrated temperature and CO_2 diffusion for the specimen, and also reduced focus instability. One image per well was acquired at 10-minute intervals, over a 12-hour period. Alternatively, transfected cells growing on 24-well or 96-well Essen Imagelock™ plates were wounded using a wound-making tool (Essen) 60 hours post transfection, cell debris was washed off and cells were incubated in migration medium alone or migration medium containing 10 ng/ml HGF. Plates were incubated in the IncuCyte™ automated imaging system and pictures were taken every 30 minutes over a 12-hour time period.

Cell tracking

Images for each condition generated using time-lapse microscopy were stacked to create movies. Movies were produced in MetaMorph software (Molecular Devices) using Codec compression. Where pictures had been taken using the IncuCyte™ system, movies were generated using the IncuCyte™ software. Cell tracks were obtained manually using the CellTracker software (Kinetic Imaging Ltd), which recorded the migration patterns of individual cells. At least 40 cells were tracked per condition. Each experiment was performed on three independent occasions. The cell tracking measurements were incorporated into a custom made journal (created by Dr Daniel Zicha) in Mathematica 5.2 software (Wolfram Research), which provided speed measurement expressed in micrometers per hour (µm/h). Motility values were normalised to those obtained from control treated cells transfected with non-targeting control siRNA (NTC). In the case of ERK rescue experiments in HeLa-cells, only GFP-positive cells were tracked.

Transwell assays

Cell migration was also assessed using an 8 µm pore 24-well format Transwell chamber assay (Becton Dickinson Discovery Labware, Bedford, MA). Cells were transfected using a reverse transfection protocol in 24-well plates. Seventy-two hours after the transfection, cells were harvested and resuspended in growth medium (GIBCO® GlutaMAX™ medium supplemented with 10% FBS). A 100 µl cell suspension was added to the top of each transwell chamber and cells were allowed to migrate for 3 hours. Lower chambers contained growth medium alone or growth medium supplemented with 10 ng/ml HGF. Each condition was carried out in duplicates. Additionally 100 µl of cell suspensions were plated onto normal 24-well plates, containing growth medium alone or growth medium supplemented with HGF. Following the migration time course, cells were resuspended with EDTA and the number of cells in the lower chamber was quantified with Cell Titer-Glo® (Promega). Additionally, the number of cells plated on the 24-well plates was quantified and the ratio of migrated cells was calculated.

Calculation of HGF migration scores

For wound healing assays, tracking experiments and transwell assays carried out when only comparing a small number of siRNAs, the fold migration was calculated by dividing the migration value obtained from HGF treated cells by the

Journal of Cell Science

value obtained from control treated cells. The migration score for a given library siRNA was calculated as follows: $(FOLD_{lib}-1)/(FOLD_{NTC}-1)$.

Immunoblotting

Transfected cells were harvested in 1× NuPAGE sample buffer (Invitrogen) 48 or 72 hours post transfection and separated on NuPAGE 4–12% gradient polyacrylamide gels according to manufacturer's instructions. Separated proteins were transferred onto a methanol-activated PVDF membrane and detected using the following primary antibodies: ERK1/2 (Santa Cruz Biotechnology), P-MET (Cell Signaling), P-ERK1/2 (Cell Signaling), MET (Santa Cruz Biotechnology), Tubulin (Sigma), Paxillin (Santa Cruz), P-Paxillin (Abcam), P-S-GSK3 (Cell Signaling), P-Y-GSK3 (Santa Cruz). Detection was carried out employing ECL, with visualisation using Hyperfilm (Amersham Biosciences) or with the ImageQuantTM LAS 4000 mini system for quantitation (GE Healthcare). Densitometric analysis of immunoblots within the linear range was performed using Image J 1.38×software (Wayne Rasband, National Institutes of Health, Bethesda, MD). Background values were subtracted, and obtained values were normalised to the tubulin loading control.

Monitoring of paxillin turnover

HeLa cells growing on glass bottom dishes were transfected with GFP-tagged paxillin and two days later either incubated in 10% FCS or 10% FCS plus 20 ng/ml HGF. Live cell imaging was performed using total internal reflection fluorescence (TIRF) microscopy. Pictures were taken every minute over a 30-minute time period. The resulting movies were used to determine the assembly and disassembly rates of paxillin-containing focal adhesions as described in (Berginski et al., 2011), using the focal adhesion analysis server (http://faas.bme.unc.edu/). Data derived from at least ten different movies were analysed. Only rates derived from curvefits with $R^2>0.75$ were included in the analysis.

Statistical analysis

Statistical significance was assessed by paired Student's *t*-test, one-way Anova or two-way Anova followed by Bonferroni post hoc test. $*P<0.05$, $**P<0.01$, $***P<0.001$; ns, not significant.

Acknowledgements

We thank the High-Throughput Screening Laboratory and the Light Microscopy Laboratory at the LRI for help with the live-cell imaging and the Nikon Imaging Centre at the Institut Curie-CNRS for their help with the TIRF microscopy experiments.

Author contributions

S.R. and M.D.R. designed the screen, S.R. wrote the manuscript, S.R. and M.M. carried out the primary screen and hit validation, C.R. carried out the TIRF experiments, S.L., C.R. and A.H. contributed to the set up of the transwell assays and live cell imaging, S.K. and P.P. supervised the project and edited the manuscript.

Funding

This work was supported by Cancer Research UK; the Deutsche Forschungsgemeinschaft (DFG) [grant number RA 1595/1-1]; and the British Lung Foundation.

Supplementary material available online at
http://jcs.biologists.org/lookup/suppl/doi:10.1242/jcs.115832/-/DC1

References

Berginski, M. E., Vitriol, E. A., Hahn, K. M. and Gomez, S. M. (2011). High-resolution quantification of focal adhesion spatiotemporal dynamics in living cells. *PLoS ONE* **6**, e22025.

Blasco, R. B., Francoz, S., Santamaría, D., Cañamero, M., Dubus, P., Charron, J., Baccarini, M. and Barbacid, M. (2011). c-Raf, but not B-Raf, is essential for development of K-Ras oncogene-driven non-small cell lung carcinoma. *Cancer Cell* **19**, 652-663.

Boeckeler, K., Rosse, C., Howell, M. and Parker, P. J. (2010). Manipulating signal delivery - plasma-membrane ERK activation in aPKC-dependent migration. *J. Cell Sci.* **123**, 2725-2732.

Bowers, D. C., Fan, S., Walter, K. A., Abounader, R., Williams, J. A., Rosen, E. M. and Laterra, J. (2000). Scatter factor/hepatocyte growth factor protects against cytotoxic death in human glioblastoma via phosphatidylinositol 3-kinase- and AKT-dependent pathways. *Cancer Res.* **60**, 4277-4283.

Brown, M. C. and Turner, C. E. (2004). Paxillin: adapting to change. *Physiol. Rev.* **84**, 1315-1339.

Cai, X., Li, M., Vrana, J. and Schaller, M. D. (2006). Glycogen synthase kinase 3- and extracellular signal-regulated kinase-dependent phosphorylation of paxillin regulates cytoskeletal rearrangement. *Mol. Cell. Biol.* **26**, 2857-2868.

Cappuzzo, F., Marchetti, A., Skokan, M., Rossi, E., Gajapathy, S., Felicioni, L., Del Grammastro, M., Sciarrotta, M. G., Buttitta, F., Incarbone, M. et al. (2009). Increased MET gene copy number negatively affects survival of surgically resected non-small-cell lung cancer patients. *J. Clin. Oncol.* **27**, 1667-1674.

Cipriani, N. A., Abidoye, O. O., Vokes, E. and Salgia, R. (2009). MET as a target for treatment of chest tumors. *Lung Cancer* **63**, 169-179.

Cross, D. A., Alessi, D. R., Cohen, P., Andjelkovich, M. and Hemmings, B. A. (1995). Inhibition of glycogen synthase kinase-3 by insulin mediated by protein kinase B. *Nature* **378**, 785-789.

Frémin, C., Bessard, A., Ezan, F., Gailhouste, L., Régeard, M., Le Seyec, J., Gilot, D., Pagès, G., Pouysségur, J., Langouët, S. et al. (2009). Multiple division cycles and long-term survival of hepatocytes are distinctly regulated by extracellular signal-regulated kinases ERK1 and ERK2. *Hepatology* **49**, 930-939.

Friedl, P. and Wolf, K. (2003). Tumour-cell invasion and migration: diversity and escape mechanisms. *Nat. Rev. Cancer* **3**, 362-374.

Gao, C. F. and Vande Woude, G. F. (2005). HGF/SF-Met signaling in tumor progression. *Cell Res.* **15**, 49-51.

Gaudino, G., Follenzi, A., Naldini, L., Collesi, C., Santoro, M., Gallo, K. A., Godowski, P. J. and Comoglio, P. M. (1994). RON is a heterodimeric tyrosine kinase receptor activated by the HGF homologue MSP. *EMBO J.* **13**, 3524-3532.

Huang, C., Jacobson, K. and Schaller, M. D. (2004). MAP kinases and cell migration. *J. Cell Sci.* **117**, 4619-4628.

Ishibe, S., Joly, D., Zhu, X. and Cantley, L. G. (2003). Phosphorylation-dependent paxillin-ERK association mediates hepatocyte growth factor-stimulated epithelial morphogenesis. *Mol. Cell* **12**, 1275-1285.

Ishibe, S., Joly, D., Liu, Z. X. and Cantley, L. G. (2004). Paxillin serves as an ERK-regulated scaffold for coordinating FAK and Rac activation in epithelial morphogenesis. *Mol. Cell* **16**, 257-267.

Jagadeeswaran, R., Surawska, H., Krishnaswamy, S., Janamanchi, V., Mackinnon, A. C., Seiwert, T. Y., Loganathan, S., Kanteti, R., Reichman, T., Nallasura, V. et al. (2008). Paxillin is a target for somatic mutations in lung cancer: implications for cell growth and invasion. *Cancer Res.* **68**, 132-142.

Karihaloo, A., O'Rourke, D. A., Nickel, C., Spokes, K. and Cantley, L. G. (2001). Differential MAPK pathways utilized for HGF- and EGF-dependent renal epithelial morphogenesis. *J. Biol. Chem.* **276**, 9166-9173.

Kermorgant, S. and Parker, P. J. (2008). Receptor trafficking controls weak signal delivery: a strategy used by c-Met for STAT3 nuclear accumulation. *J. Cell Biol.* **182**, 855-863.

Kermorgant, S., Zicha, D. and Parker, P. J. (2004). PKC controls HGF-dependent c-Met traffic, signalling and cell migration. *EMBO J.* **23**, 3721-3734.

Lefloch, R., Pouysségur, J. and Lenormand, P. (2008). Single and combined silencing of ERK1 and ERK2 reveals their positive contribution to growth signaling depending on their expression levels. *Mol. Cell. Biol.* **28**, 511-527.

Lefloch, R., Pouysségur, J. and Lenormand, P. (2009). Total ERK1/2 activity regulates cell proliferation. *Cell Cycle* **8**, 705-711.

Liu, Z. X., Yu, C. F., Nickel, C., Thomas, S. and Cantley, L. G. (2002). Hepatocyte growth factor induces ERK-dependent paxillin phosphorylation and regulates paxillin-focal adhesion kinase association. *J. Biol. Chem.* **277**, 10452-10458.

Ma, P. C., Jagadeeswaran, R., Jagadeesh, S., Tretiakova, M. S., Nallasura, V., Fox, E. A., Hansen, M., Schaefer, E., Naoki, K., Lader, A. et al. (2005). Functional expression and mutations of c-Met and its therapeutic inhibition with SU11274 and small interfering RNA in non-small cell lung cancer. *Cancer Res.* **65**, 1479-1488.

Ma, P. C., Tretiakova, M. S., MacKinnon, A. C., Ramnath, N., Johnson, C., Dietrich, S., Seiwert, T., Christensen, J. G., Jagadeeswaran, R., Krausz, T. et al. (2008). Expression and mutational analysis of MET in human solid cancers. *Genes Chromosomes Cancer* **47**, 1025-1037.

Mackinnon, A. C., Tretiakova, M., Henderson, L., Mehta, R. G., Yan, B. C., Joseph, L., Krausz, T., Husain, A. N., Reid, M. E. and Salgia, R. (2011). Paxillin expression and amplification in early lung lesions of high-risk patients, lung adenocarcinoma and metastatic disease. *J. Clin. Pathol.* **64**, 16-24.

Marchi, M., D'Antoni, A., Formentini, I., Parra, R., Brambilla, R., Ratto, G. M. and Costa, M. (2008). The N-terminal domain of ERK1 accounts for the functional differences with ERK2. *PLoS ONE* **3**, e3873.

Menakongka, A. and Suthiphongchai, T. (2010). Involvement of PI3K and ERK1/2 pathways in hepatocyte growth factor-induced cholangiocarcinoma cell invasion. *World J. Gastroenterol.* **16**, 713-722.

Miller, C. T., Lin, L., Casper, A. M., Lim, J., Thomas, D. G., Orringer, M. B., Chang, A. C., Chambers, A. F., Giordano, T. J., Glover, T. W. et al. (2006). Genomic amplification of MET with boundaries within fragile site FRA7G and upregulation of MET pathways in esophageal adenocarcinoma. *Oncogene* **25**, 409-418.

Peruzzi, B. and Bottaro, D. P. (2006). Targeting the c-Met signaling pathway in cancer. *Clin. Cancer Res.* **12**, 3657-3660.

Potempa, S. and Ridley, A. J. (1998). Activation of both MAP kinase and phosphatidylinositide 3-kinase by Ras is required for hepatocyte growth factor/scatter factor-induced adherens junction disassembly. *Mol. Biol. Cell* **9**, 2185-2200.

Ronsin, C., Muscatelli, F., Mattei, M. G. and Breathnach, R. (1993). A novel putative receptor protein tyrosine kinase of the met family. *Oncogene* **8**, 1195-1202.

Sattler, M. and Salgia, R. (2007). c-Met and hepatocyte growth factor: potential as novel targets in cancer therapy. *Curr. Oncol. Rep.* **9**, 102-108.

Sattler, M., Reddy, M. M., Hasina, R., Gangadhar, T. and Salgia, R. (2011). The role of the c-Met pathway in lung cancer and the potential for targeted therapy. *Ther Adv. Med. Oncol.* **3**, 171-184.

Shin, S., Dimitri, C. A., Yoon, S. O., Dowdle, W. and Blenis, J. (2010). ERK2 but not ERK1 induces epithelial-to-mesenchymal transformation via DEF motif-dependent signaling events. *Mol. Cell* **38**, 114-127.

Srinivasan, R., Zabuawala, T., Huang, H., Zhang, J., Gulati, P., Fernandez, S., Karlo, J. C., Landreth, G. E., Leone, G. and Ostrowski, M. C. (2009). Erk1 and Erk2 regulate endothelial cell proliferation and migration during mouse embryonic angiogenesis. *PLoS ONE* **4**, e8283.

Tanimura, S., Chatani, Y., Hoshino, R., Sato, M., Watanabe, S., Kataoka, T., Nakamura, T. and Kohno, M. (1998). Activation of the 41/43 kDa mitogen-activated protein kinase signaling pathway is required for hepatocyte growth factor-induced cell scattering. *Oncogene* **17**, 57-65.

Tanimura, S., Nomura, K., Ozaki, K., Tsujimoto, M., Kondo, T. and Kohno, M. (2002). Prolonged nuclear retention of activated extracellular signal-regulated kinase 1/2 is required for hepatocyte growth factor-induced cell motility. *J. Biol. Chem.* **277**, 28256-28264.

Tong, C. Y., Hui, A. B., Yin, X. L., Pang, J. C., Zhu, X. L., Poon, W. S. and Ng, H. K. (2004). Detection of oncogene amplifications in medulloblastomas by comparative genomic hybridization and array-based comparative genomic hybridization. *J. Neurosurg.* **100 Suppl Pediatrics**, 187-193.

Trusolino, L., Bertotti, A. and Comoglio, P. M. (2010). MET signalling: principles and functions in development, organ regeneration and cancer. *Nat. Rev. Mol. Cell Biol.* **11**, 834-848.

Vantaggiato, C., Formentini, I., Bondanza, A., Bonini, C., Naldini, L. and Brambilla, R. (2006). ERK1 and ERK2 mitogen-activated protein kinases affect Ras-dependent cell signaling differentially. *J. Biol.* **5**, 14.

Vicente-Manzanares, M., Webb, D. J. and Horwitz, A. R. (2005). Cell migration at a glance. *J. Cell Sci.* **118**, 4917-4919.

Voisin, L., Saba-El-Leil, M. K., Julien, C., Frémin, C. and Meloche, S. (2010). Genetic demonstration of a redundant role of extracellular signal-regulated kinase 1 (ERK1) and ERK2 mitogen-activated protein kinases in promoting fibroblast proliferation. *Mol. Cell. Biol.* **30**, 2918-2932.

von Thun, A., Birtwistle, M., Kalna, G., Grindlay, J., Strachan, D., Kolch, W., von Kriegsheim, A. and Norman, J. C. (2012). ERK2 drives tumour cell migration in 3D microenvironments by suppressing expression of Rab17 and Liprin-beta2. *J. Cell Sci.* **125**, 1465-1477.

Wang, Q. M., Fiol, C. J., DePaoli-Roach, A. A. and Roach, P. J. (1994). Glycogen synthase kinase-3 beta is a dual specificity kinase differentially regulated by tyrosine and serine/threonine phosphorylation. *J. Biol. Chem.* **269**, 14566-14574.

Webb, D. J., Donais, K., Whitmore, L. A., Thomas, S. M., Turner, C. E., Parsons, J. T. and Horwitz, A. F. (2004). FAK-Src signalling through paxillin, ERK and MLCK regulates adhesion disassembly. *Nat. Cell Biol.* **6**, 154-161.

Webb, D. J., Schroeder, M. J., Brame, C. J., Whitmore, L., Shabanowitz, J., Hunt, D. F. and Horwitz, A. R. (2005). Paxillin phosphorylation sites mapped by mass spectrometry. *J. Cell Sci.* **118**, 4925-4929.

Wu, D. W., Cheng, Y. W., Wang, J., Chen, C. Y. and Lee, H. (2010). Paxillin predicts survival and relapse in non-small cell lung cancer by microRNA-218 targeting. *Cancer Res.* **70**, 10392-10401.

Zeigler, M. E., Chi, Y., Schmidt, T. and Varani, J. (1999). Role of ERK and JNK pathways in regulating cell motility and matrix metalloproteinase 9 production in growth factor-stimulated human epidermal keratinocytes. *J. Cell. Physiol.* **180**, 271-284.

Zhang, Y. W., Wang, L. M., Jove, R. and Vande Woude, G. F. (2002). Requirement of Stat3 signaling for HGF/SF-Met mediated tumorigenesis. *Oncogene* **21**, 217-226.

Journal of Cell Science